

Parity nonconserving observables in thermal neutron capture on a proton

C. H. Hyun^{a, b*}, S. J. Lee^a, J. Haidenbauer^c, S. W. Hong^a

(a) *Department of Physics and Institute of Basic Science,*

Sungkyunkwan University, Suwon 440-746, Korea

(b) *School of Physics, Seoul Nat'l University, Seoul 151-742, Korea*

(c) *Forschungszentrum Jülich, Institut für Kernphysik, D-52425 Jülich, Germany*

(Dated: November 26, 2004)

Abstract

We calculate parity nonconserving observables in the processes where a neutron is captured on a proton at the threshold energy radiating a photon. Various potential models such as Paris, Bonn and Argonne *v*18 are used for the strong interactions, and the meson-exchange description is employed for the weak interactions between hadrons. The photon polarization P_γ in the unpolarized neutron capture process and photon asymmetry A_γ in the polarized neutron capture process are obtained in terms of the weak meson-nucleon coupling constants. A_γ turns out to be basically insensitive to the employed strong interaction models and thus can be uniquely determined in terms of the weak coupling constants, but P_γ depends significantly on the strong interaction models.

* e-mail: hch@meson.skku.ac.kr

I. INTRODUCTION

Recent experiments to explore the weak interactions between hadrons through parity nonconserving (PNC) observables in nuclear systems [1, 2] or reactions [3, 4] have triggered revived interests in this field. These PNC observables can be related to the meson-nucleon weak coupling constants which are introduced in the meson-exchange potential description of the hadronic weak interaction [5]. However, due to various uncertainties (see Ref. [5] for details), the weak coupling constants were fixed only within certain ranges [5]. Thus, it has been hoped that the PNC observables from various experiments can reduce the range of these coupling constants and eventually determine the values. The situation, however, has not been much improved even by the recent measurements. For example, the value of the $\pi - N$ weak coupling constant, h_π^1 , from the anapole moment of ^{133}Cs [1] is inconsistent with a previous value obtained from the forbidden γ -decay of ^{18}F [6]: h_π^1 determined by the former is larger than that from the latter by a factor of 7. New experiments, already completed [3], being done [4] or expected to be performed, concern two-nucleon systems in which many body effects are absent. Thus they are expected to give more stringent constraints on the weak coupling constants. For the current status of research on the weak coupling constants, see [7].

In this work, we calculate the photon asymmetry A_γ in the radiative capture of a polarized neutron on a proton, $\vec{n} + p \rightarrow d + \gamma$, and the circular polarization of photons P_γ in $n + p \rightarrow d + \gamma$ at the threshold. The latest experimental value of A_γ is $-(1.5 \pm 4.8) \times 10^{-8}$ [8], but the experiment being done at LANSCE aims at the accuracy of 10^{-9} [4]. Theoretical calculations of A_γ using strong models made in the 1960's and the 1970's such as Hamada-Johnston, Reid-soft-core and Tourreil-Sprung show results similar to each other; $A_\gamma \simeq -0.11h_\pi^1$ [9]. A_γ is predominantly determined by h_π^1 and depends very little on other coupling constants (as will be shown in Table I). In this work we present A_γ calculated with potentials such as Paris [10], Bonn [11], Bonn-A and Bonn-B [12], and Argonne $v18$ (Av18) [13]. We compare our results with previous ones [9] and investigate the model dependence of A_γ .

Contrary to A_γ , P_γ at the threshold is known to be sensitive to the heavy meson (ρ and ω) components of the weak potentials [9, 14]. The most recent experimental value of P_γ is $(1.8 \pm 1.8) \times 10^{-7}$ [15], and theoretical calculations made in the 1970's agree with this value within the experimental errors. However, since P_γ is sensitive to the short range properties

of the strong interactions as well as of the weak interactions, its model dependence is more noticeable than A_γ [14, 16]. Since the inverse process, $\vec{\gamma} + d \rightarrow n + p$, whose PNC asymmetry at the threshold is equal to P_γ , becomes experimentally feasible nowadays, we expect that P_γ can be measured more precisely and can provide more constraints on the weak dynamics of hadrons. We thus investigate the model dependence of P_γ with the same potentials that we use in calculating A_γ .

In Sect. 2, we present the Desplanques-Donaghue-Holstein (DDH) potential [5] and the parity-admixed wave functions in the initial and the final states. In Sect. 3, the electromagnetic operators are presented, matrix elements are derived, and the results for A_γ and P_γ are shown. Discussions on the results follow in Sect. 4.

II. PARITY ADMIXED WAVE FUNCTION

The Schrödinger equation for a two-nucleon system can be written as

$$\begin{aligned} H \Psi(\mathbf{r}) &= \left[-\frac{1}{m_N} \left(\frac{1}{r} \frac{\partial^2}{\partial r^2} r - \frac{l(l+1)}{r^2} \right) + V_C(r) + V_T(r) S_{12}(\hat{\mathbf{r}}) + V_{pnc}(\mathbf{r}) \right] \Psi(\mathbf{r}) \\ &= E \Psi(\mathbf{r}), \end{aligned} \quad (1)$$

where V_T represents the tensor potential and V_C includes central, spin-orbit, spin-spin and quadratic spin-orbit interactions in the strong potential. In the Paris and Bonn potentials, it is essential to include the momentum dependent term in the central potential to obtain the correct phase shifts even at low energies. In Ref. [17] a transformation useful for treating the momentum dependent term is suggested. In this work, however, we have dealt with the momentum dependent terms without using such a transformation and have solved the Schrödinger equation as it is. We have confirmed that the solutions thus obtained reproduce the results of each potential model [10, 11, 12] fairly well with differences less than 1%. The small differences can be attributed to the use of slightly different values of physical quantities in the calculations. V_{pnc} is the PNC potential, and we use the one given by DDH [5]

$$\begin{aligned} V_{pnc}(\mathbf{r}) &= V_{pnc}^\pi(\mathbf{r}) + V_{pnc}^\rho(\mathbf{r}) + V_{pnc}^\omega(\mathbf{r}), \\ V_{pnc}^\pi(\mathbf{r}) &= i \frac{g_{\pi NN} h_\pi^1}{2\sqrt{2}m_N} (\boldsymbol{\tau}_1 \times \boldsymbol{\tau}_2)^z (\boldsymbol{\sigma}_1 + \boldsymbol{\sigma}_2) \cdot [\mathbf{p}, f_\pi(r)], \\ V_{pnc}^\rho(\mathbf{r}) &= -\frac{g_{\rho NN}}{m_N} \left[\left(h_\rho^0 \boldsymbol{\tau}_1 \cdot \boldsymbol{\tau}_2 + \frac{1}{2} h_\rho^1 (\tau_1^z + \tau_2^z) + \frac{h_\rho^2}{2\sqrt{6}} (3\tau_1^z \tau_2^z - \boldsymbol{\tau}_1 \cdot \boldsymbol{\tau}_2) \right) \times \right. \end{aligned} \quad (2)$$

$$\begin{aligned}
& \left((\boldsymbol{\sigma}_1 - \boldsymbol{\sigma}_2) \cdot \{\mathbf{p}, f_\rho(r)\} + i(1 + \chi_\rho) (\boldsymbol{\sigma}_1 \times \boldsymbol{\sigma}_2) \cdot [\mathbf{p}, f_\rho(r)] \right) \\
& + i \frac{h_\rho^{1'}}{2} (\boldsymbol{\tau}_1 \times \boldsymbol{\tau}_2)^z (\boldsymbol{\sigma}_1 + \boldsymbol{\sigma}_2) \cdot [\mathbf{p}, f_\rho(r)] - \frac{h_\rho^1}{2} (\tau_1^z - \tau_2^z) (\boldsymbol{\sigma}_1 + \boldsymbol{\sigma}_2) \cdot \{\mathbf{p}, f_\rho(r)\} \Big], \quad (3) \\
V_{pnc}^\omega(\mathbf{r}) &= -\frac{g_{\omega NN}}{m_N} \left[\left(h_\omega^0 + \frac{1}{2} h_\omega^1 (\tau_1^z + \tau_2^z) \right) \times \right. \\
& \left((\boldsymbol{\sigma}_1 - \boldsymbol{\sigma}_2) \cdot \{\mathbf{p}, f_\omega(r)\} + i(1 + \chi_\omega) (\boldsymbol{\sigma}_1 \times \boldsymbol{\sigma}_2) \cdot [\mathbf{p}, f_\omega(r)] \right) \\
& \left. + \frac{h_\omega^1}{2} (\tau_1^z - \tau_2^z) (\boldsymbol{\sigma}_1 + \boldsymbol{\sigma}_2) \cdot \{\mathbf{p}, f_\omega(r)\} \right], \quad (4)
\end{aligned}$$

where the strong coupling constants are $g_{\pi NN} = 13.45$, $g_{\rho NN} = 2.79$, $g_{\omega NN} = 8.37$ and the anomalous magnetic moments are $\chi_\rho = 3.71$ and $\chi_\omega = -0.12$. The Yukawa functions $f_M(r)$ are defined as

$$f_M(r) = \frac{e^{-m_M r}}{4\pi r}, \quad (M = \pi, \rho, \omega).$$

The quantities $h_M^{\Delta I}$ represent the weak meson-nucleon coupling constants where ΔI denotes the isospin transfer.

At the threshold energy, the initial scattering state, $n + p$, is dominated by the lowest angular momentum state, i.e., the 1S_0 channel, and higher angular momentum states are suppressed. Thus in this work we just include the next low-lying state, the ${}^3S_1 - {}^3D_1$ partial waves, where the 3D_1 state is induced by the tensor interaction in the initial scattering state. Then the parity-even state of the initial wave function consists of the 1S_0 , 3S_1 and 3D_1 states.

Since V_{pnc} is a parity-odd operator, it creates opposite parity components in the wave function. For example, when V_{pnc} is operated on the 1S_0 state, the isoscalar and isotensor terms of V_{pnc} generate a ${}^3\tilde{P}_0$ admixture, where the tilde denotes the parity-admixed components generated from the DDH potential. Similarly, ${}^3\tilde{P}_1$ and ${}^1\tilde{P}_1$ admixtures arise from applying the isovector and isoscalar components of V_{pnc} to the ${}^3S_1 - {}^3D_1$ state, respectively. The total wave function of the initial state with its parity admixture at the threshold can be written as

$$\begin{aligned}
\Psi_i(\mathbf{r}) &= \Psi_i^{pc}(\mathbf{r}) + \Psi_i^{pnc}(\mathbf{r}), \\
\Psi_i^{pc}(\mathbf{r}) &= \frac{1}{\sqrt{4\pi r}} \left[u_s(r) \chi_{00} \zeta_{10} + \left(u_t(r) + \frac{S_{12}(\hat{\mathbf{r}})}{\sqrt{8}} w_t(r) \right) \chi_{1S_z} \zeta_{00} \right], \quad (5)
\end{aligned}$$

$$\Psi_i^{pnc}(\mathbf{r}) = -\frac{i}{\sqrt{4\pi r}} \left[\sqrt{\frac{3}{8}} \tilde{v}_t^{3p1}(r) (\boldsymbol{\sigma}_1 + \boldsymbol{\sigma}_2) \chi_{1S_z} \zeta_{10} + \frac{1}{2} \tilde{v}_t^{3p0}(r) (\boldsymbol{\sigma}_1 - \boldsymbol{\sigma}_2) \chi_{00} \zeta_{10} \right] \cdot \hat{\mathbf{r}}, \quad (6)$$

where χ_{SS_z} and ζ_{TT_z} represent the spin and isospin part, respectively. u_s is the radial part of the wave function for the 1S_0 channel, u_t for 3S_1 and w_t for 3D_1 . The final state wave function can be written in a similar way as

$$\Psi_f(\mathbf{r}) = \Psi_f^{pc}(\mathbf{r}) + \Psi_f^{pnc}(\mathbf{r}),$$

$$\Psi_f^{pc}(\mathbf{r}) = \frac{1}{\sqrt{4\pi}r} \left(u_d(r) + \frac{S_{12}(\hat{\mathbf{r}})}{\sqrt{8}} w_d(r) \right) \chi_{1S_z} \zeta_{00}, \quad (7)$$

$$\Psi_f^{pnc}(\mathbf{r}) = \frac{i}{\sqrt{4\pi}r} \left[\frac{\sqrt{3}}{2} \tilde{v}_d^{1p1}(r) (\boldsymbol{\sigma}_1 - \boldsymbol{\sigma}_2) \chi_{1S_z} \zeta_{00} - \sqrt{\frac{3}{8}} \tilde{v}_d^{3p1}(r) (\boldsymbol{\sigma}_1 + \boldsymbol{\sigma}_2) \chi_{1S_z} \zeta_{10} \right] \cdot \hat{\mathbf{r}}, \quad (8)$$

where $u_d(r)$ ($w_d(r)$) is the radial wave function for the 3S_1 (3D_1) deuteron state, and \tilde{v}_d^{1p1} and \tilde{v}_d^{3p1} denote the parity nonconserving admixture due to the $^1\tilde{P}_1$ and $^3\tilde{P}_1$ states, respectively. By inserting the initial and the final wave functions into the Schrödinger equation (1) with the strong and weak PNC potentials, one can obtain the radial wave equation for each channel (see Appendix for details).

III. MATRIX ELEMENTS, P_γ AND A_γ

At the threshold energy, it is well known that the neutron capture cross section is dominated by the isovector M1 transition. We can evaluate the parity conserving M1 transition amplitude by using the one-body spin current operator

$$\mathbf{J}_M = -i \frac{\mu_V}{4m_N} \sum_i \tau_i^z \boldsymbol{\sigma}_i \times \mathbf{k}_\gamma, \quad (9)$$

where $\mu_V = 4.71$, and \mathbf{k}_γ is the photon momentum. Amplitudes between the states with opposite parities would become non-zero through the E1 transition. While the impulse approximation is used in evaluating the M1 amplitude, the contribution from the exchange currents can be well accounted for by the Siegert's theorem. The E1 current operator with Siegert's theorem reads

$$\mathbf{J}_E^S = -i \frac{\omega}{4} (\tau_1^z - \tau_2^z) \mathbf{r}, \quad (10)$$

where ω is the photon energy (2.2246 MeV at threshold). The transition amplitudes (\mathcal{M}_i^f) can be classified in terms of the electromagnetic type \mathcal{M} ($=M$ or E), the initial (i) and the final (f) states. The leading parity-conserving isovector M1 transition occurs between the initial 1S_0 and final 3S_1 states, and we denote its amplitude by M_{1s0}^{3s1} . The non-zero PNC E1 amplitudes are represented similarly as \tilde{E}_{3p0}^{3s1} for $^3\tilde{P}_0 \rightarrow ^3S_1 + ^3D_1$, \tilde{E}_{1s0}^{1p1} for $^1S_0 \rightarrow ^1\tilde{P}_1$,

\tilde{E}_{3p1}^{3s1} for ${}^3\tilde{P}_1 \rightarrow {}^3S_1 + {}^3D_1$, and \tilde{E}_{3s1}^{3p1} for ${}^3S_1 + {}^3D_1 \rightarrow {}^3\tilde{P}_1$, where the tildes are to distinguish the PNC amplitudes from the normal parity conserving ones. With the wave functions of Eqs. (5)–(8), we obtain the matrix elements

$$M_{1s0}^{3s1} = \frac{\omega \mu_V}{4m_N} \int dr u_d(r) u_s(r), \quad (11)$$

$$\tilde{E}_{3p0}^{3s1} = \frac{\omega}{12} \int dr r (u_d(r) - \sqrt{2}w_d(r)) \tilde{v}_t^{3p0}(r), \quad (12)$$

$$\tilde{E}_{1s0}^{1p1} = \frac{\omega}{4\sqrt{3}} \int dr r \tilde{v}_d^{1p1}(r) u_s(r), \quad (13)$$

$$\tilde{E}_{3p1}^{3s1} = -\frac{\omega}{4\sqrt{6}} \int dr r \left(u_d(r) + \frac{w_d(r)}{\sqrt{2}} \right) \tilde{v}_t^{3p1}, \quad (14)$$

$$\tilde{E}_{3s1}^{3p1} = \frac{\omega}{4\sqrt{6}} \int dr r \tilde{v}_d^{3p1} \left(u_t(r) + \frac{w_t(r)}{\sqrt{2}} \right). \quad (15)$$

In terms of these electromagnetic amplitudes, the two PNC observables are written as

$$A_\gamma = -2 \frac{\tilde{E}_{3p1}^{3s1} + \tilde{E}_{3s1}^{3p1}}{M_{1s0}^{3s1}} \equiv A_\gamma^i + A_\gamma^f, \quad (16)$$

$$P_\gamma = -2 \frac{\tilde{E}_{3p0}^{3s1} + \tilde{E}_{1s0}^{1p1}}{M_{1s0}^{3s1}} \equiv P_\gamma^i + P_\gamma^f, \quad (17)$$

where $A_\gamma^i \equiv -2\tilde{E}_{3p1}^{3s1}/M_{1s0}^{3s1}$ and $P_\gamma^i \equiv -2\tilde{E}_{3p0}^{3s1}/M_{1s0}^{3s1}$ have the PNC component in the initial state and $A_\gamma^f \equiv -2\tilde{E}_{3s1}^{3p1}/M_{1s0}^{3s1}$ and $P_\gamma^f \equiv -2\tilde{E}_{1s0}^{1p1}/M_{1s0}^{3s1}$ have the PNC component in the final state. Numerical results are given in Table I. We express the results for A_γ and P_γ in terms of the weak coupling constants $h_M^{\Delta I}$ to show explicitly the dependence of A_γ and P_γ on each meson. “Best values” refer to A_γ and P_γ values evaluated with the so-called best values of the weak meson-coupling constants suggested by Ref. [5]. They are $h_\rho^0 = -11.4$, $h_\omega^0 = -1.9$, $h_\rho^2 = -9.5$, $h_\pi^1 = 4.6$, $h_\rho^1 = -0.2$ and $h_\omega^1 = -1.1$, in units of 10^{-7} .

IV. RESULTS AND DISCUSSIONS

Asymmetry (A_γ)

As shown in Table I, the Bonn and Av18 models predict the same A_γ value, while the best value from the Paris potential is larger in magnitude than those from Bonn and Av18 by a factor of 1.27. This factor can be understood by examining the wave functions that contribute to A_γ . u_s and u_d are plotted in Fig. 1, and \tilde{v}_d^{3p1} in Fig. 2. As can be seen in Fig. 1 and 2, u_d and \tilde{v}_d^{3p1} calculated with different potentials are very similar to each other for all potentials, but u_s calculated with the Paris potential is substantially different from u_s from

Model	A_γ	Best values ($\times 10^{-8}$)		
		A_γ	A_γ^i	A_γ^f
Paris	$-0.148h_\pi^1 - 0.001h_\rho^1 + 0.003h_\omega^1$	-6.85	-3.34	-3.51
Bonn	$-0.117h_\pi^1 - 0.001h_\rho^1 + 0.003h_\omega^1$	-5.42	-2.66	-2.76
Bonn-B	$-0.117h_\pi^1 - 0.001h_\rho^1 + 0.002h_\omega^1$	-5.41	-2.65	-2.76
Av18	$-0.117h_\pi^1 - 0.001h_\rho^1 + 0.002h_\omega^1$	-5.41	-2.63	-2.78

Model	P_γ	Best values ($\times 10^{-8}$)		
		P_γ	P_γ^i	P_γ^f
Paris	$-0.0106h_\rho^0 + 0.0074h_\omega^0 - 0.0191h_\rho^2$	2.88	-1.24	4.12
Bonn	$-0.0890h_\rho^0 + 0.0088h_\omega^0 - 0.0214h_\rho^2$	12.01	-1.40	13.4
Bonn-B	$-0.0286h_\rho^0 + 0.0012h_\omega^0 - 0.0208h_\rho^2$	5.21	-1.35	6.56
Av18	$-0.0088h_\rho^0 + 0.0034h_\omega^0 - 0.0175h_\rho^2$	2.64	-1.11	3.75

TABLE I: Results for the observables A_γ and P_γ for various phenomenological models in terms of the weak coupling constants $h_M^{\Delta I}$. Best values mean A_γ and P_γ values obtained with the best values of $h_M^{\Delta I}$ suggested by DDH. They are in units of 10^{-8} . The definitions of $P_\gamma^{i,f}$ and $A_\gamma^{i,f}$ are given in Eqs. (17) and (16), respectively.

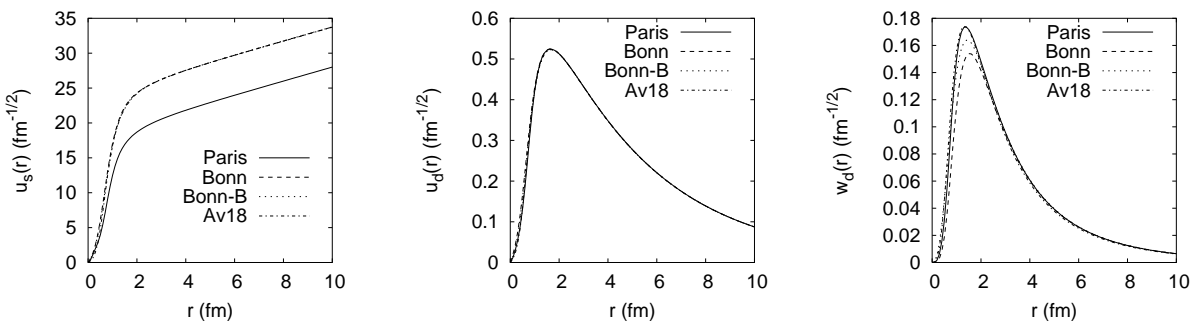


FIG. 1: The wave functions $u_s(r)$, $u_d(r)$ and $w_d(r)$ calculated with different potentials are plotted. The results for $u_s(r)$ from Bonn, Bonn-B and Av18 are indistinguishable and correspond to the upper curve in the figure. $u_t(r)$ and $w_t(r)$ are not shown here, because they do not depend very much on the models.

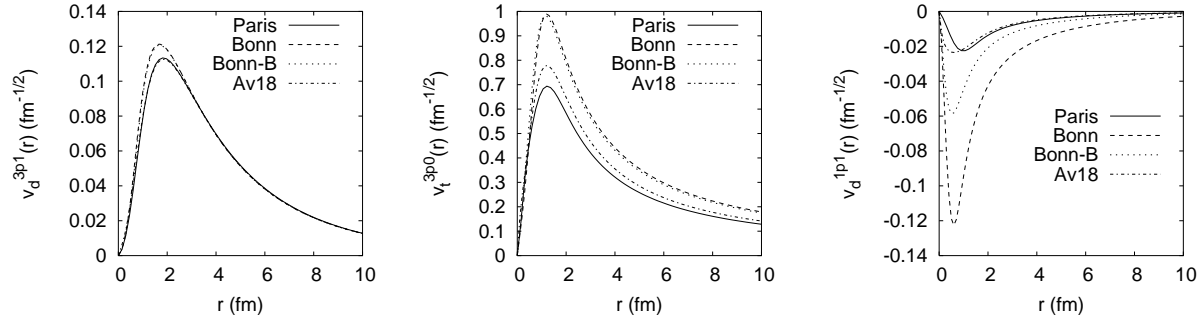


FIG. 2: Wave functions for the parity-admixed states for different potentials. The wave functions are given in units of h_π^1 . Note the difference in the scale.

other potentials. (\tilde{v}_t^{3p1} , though not shown here, is more or less the same for all potential models.) The reason for this difference can be traced back to the fact that the Paris potential was fitted to proton-proton data and therefore yields a scattering length of $a = -17.6$ fm for the 1S_0 channel (in the absence of the Coulomb interaction) while Av18 and Bonn are neutron-proton models and yield $a = -23.7$ fm. The M1 isovector amplitude M_{1s0}^{3s1} in the denominator of Eqs. (16) and (17) is 0.184 for Paris potential and 0.233 for Av18 and Bonn potentials. Since the wave functions that contribute to the E1 amplitude in Eqs. (14) and (15) (numerator of A_γ) are very similar, the difference in the values of A_γ comes mostly from the value of the M1 amplitude in the denominator of A_γ . Indeed, the ratio of the M1 amplitudes for Av18 to Paris, 1.27, is equal to the ratio of the best value of A_γ . Thus, if one could readjust the Paris potential to produce the accepted $n - p$ scattering length in the 1S_0 channel, the four models would give us essentially model-independent A_γ values. A recent work [18] in which various contributions from the exchange currents are taken into account confirms this model-independent nature of A_γ . The magnitude of A_γ in Ref. [18] ($A_\gamma = -4.98 \times 10^{-8}$) with pion-exchange currents is smaller than ours ($A_\gamma = -5.41 \times 10^{-8}$) by about 9 %, and is in agreement with the result of Ref. [19] ($A_\gamma = -4.94 \times 10^{-8}$) where one-body and leading pion-exchange currents are considered. On the other hand, if one employs the h_π^1 value from the ^{18}F [6] and ^{133}Cs [1] experiments, A_γ becomes -1.52×10^{-8} and -11.1×10^{-8} , respectively. Since the contribution from the pion to A_γ is more than 99 % of the total value (see Table I), a more accurate measurement of A_γ can provide a stringent determination of h_π^1 .

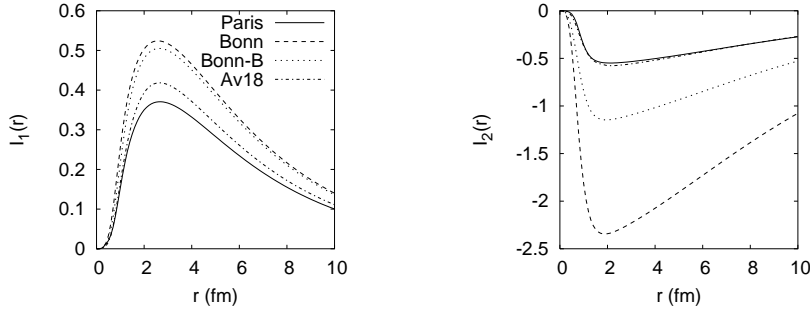


FIG. 3: Integrands that enter into the E1 amplitude of P_γ . The left panel shows $I_1(r) \equiv r(u_d(r) - \sqrt{2}w_d(r))\tilde{v}_t^{3p0}(r)$ of Eq. (12), and the right one $I_2(r) \equiv r\tilde{v}_d^{1p1}(r)u_s(r)$ of Eq. (13).

In passing, we remark that A_γ from a previous work [20] using Paris potential differs from our A_γ in sign though the magnitudes agree. It appears that the definitions of A_γ differ in sign.

Polarization (\mathbf{P}_γ)

While A_γ is dominated by the long range part of the interactions and is practically model-independent, P_γ depends strongly on the heavy meson exchanges and on the potential model. P_γ 's calculated with the best values of the weak coupling constants [5] and Paris and Av18 potentials are similar to each other, but P_γ 's evaluated with Bonn and Bonn-B are larger than that with Av18 by a factor of 5 and 2, respectively. (Bonn-A and Bonn produce similar results and thus Bonn-A is not included in the discussion.) P_γ 's expressed in terms of $h_M^{\Delta I}$ in Table I show that P_γ from Bonn is more sensitive to h_ρ^0 than P_γ from other potentials, while the terms depending on h_ω^0 and h_ρ^2 are only moderately model dependent. The contributions from the initial (${}^3\tilde{P}_0$) and the final (${}^1\tilde{P}_1$) states listed in Table I show that the initial state contribution (P_γ^i) is rather model-independent, but the contribution from the final state (P_γ^f) is highly dependent on the potentials.

The numerical factors in front of the weak coupling constants in Table I are determined by the strong potentials in each channel through the wave functions of the 1S_0 and ${}^3S_1 - {}^3D_1$ channels that enter into the source terms in the Schrödinger equation of the parity-admixed states (see Appendix). The wave functions for the ${}^3\tilde{P}_0$ and the ${}^1\tilde{P}_1$ states are shown in Fig. 2, and the corresponding integrands of the E1 amplitudes, Eqs. (12) and (13), are shown in Fig. 3. The wave function ($\tilde{v}_t^{3p0}(r)$) and the integrand ($I_1(r)$) for the ${}^3\tilde{P}_0$ state exhibit a sizeable model dependence. However, for the ${}^1\tilde{P}_1$ channel there are even more

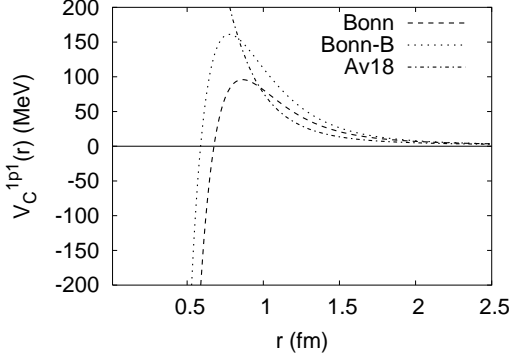


FIG. 4: Comparison of the central potentials in the 1P_1 channel of the Bonn, Bonn-B, and Av18 potentials.

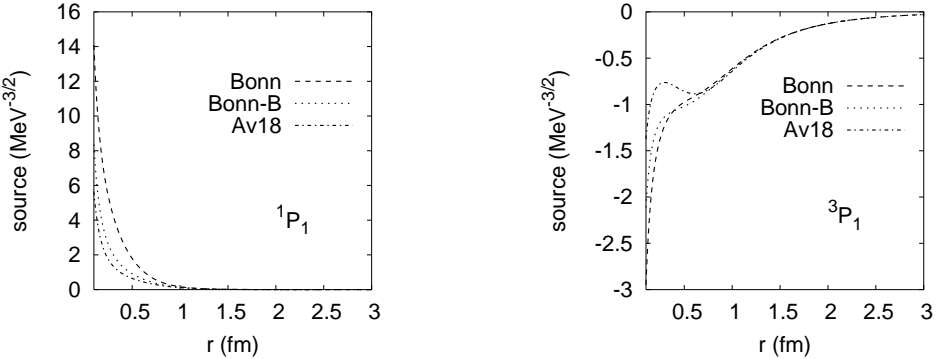


FIG. 5: Source terms for the $^1\tilde{P}_1$ and $^3\tilde{P}_1$ states. Compared to the terms of 3P_1 , those of 1P_1 are more model dependent. Note the difference in the scale.

drastic variations in both wave function ($\tilde{v}_d^{1p1}(r)$) and the integrand ($I_2(r)$) depending on different potentials. Such a strong model dependency can be understood from the behavior of the strong potential in the 1P_1 channel and the source term that contributes to \tilde{v}_d^{1p1} in the Schrödinger equation (see Eq. (A.6)). Fig. 4 shows the strong potentials in the 1P_1 channel. The Bonn potential for 1P_1 channel becomes attractive in the short range region while Av18 is repulsive in the whole region. The attraction at short ranges increases the probability for a nucleon to be present in the region, and this can partly explain the shape of \tilde{v}_d^{1p1} in Fig. 2. A recent work by R. Schiavilla *et al.* shows a similar behavior of \tilde{v}_d^{1p1} [18].

In Fig. 5, we compare the source terms of the $^3\tilde{P}_1$ (the right hand side of Eq. (A.5)) and $^1\tilde{P}_1$ (the right hand side of Eq. (A.6)) states. The sources for the $^3\tilde{P}_1$ state from different models

show a moderate model dependence for $r \leq 0.5$ fm, but they have significant magnitudes and are indistinguishable in the intermediate and long range regions, which explains the model independent results of A_γ in Table I. On the contrary, most of the contribution to the source terms of \tilde{v}_d^{1p1} comes from the intermediate and short range region, and they depend strongly on the model. A larger source combined with attraction in the short-range region, as it is the case for the ${}^1\tilde{P}_1$ channel of the Bonn models, yields an enhanced contribution to P_γ .

Concluding, we have calculated parity non-conserving observables P_γ for the reaction $n + p \rightarrow d + \gamma$ and A_γ for the reaction $\vec{n} + p \rightarrow d + \gamma$ at threshold. We have employed the Paris, Bonn and Av18 potentials for the strong interaction and the DDH potential for the weak interaction. A_γ turns out to be independent of the strong interaction models, while P_γ is sensitive to the dynamics at short ranges. Since A_γ is rather strong-interaction independent, one can reduce the uncertainty in the value of h_π^1 by measuring A_γ accurately. Regarding P_γ , there are relatively large uncertainties, which stem from ambiguities in both strong and weak interactions at short ranges. However, since the major uncertainty comes from the ${}^1\tilde{P}_1$ channel and the value of h_ρ^0 , an accurate experimental measurement of P_γ can shed some light on the weak coupling constants.

Acknowledgments

We thank B. Desplanques for useful discussions. The work is supported by the Korea Research Foundation Grant (KRF-2003-070-C00015).

APPENDIX

The radial equations for the 1S_0 continuum, and the ${}^3S_1 - {}^3D_1$ continuum and bound states read

$$u_s''(r) + m_N (E - V_C(r)) u_s(r) = 0, \quad (\text{A.1})$$

$$u_{t(d)}''(r) + m_N (E - V_C(r)) u_{t(d)}(r) = \sqrt{8}m_N V_T(r) w_{t(d)}(r), \quad (\text{A.2})$$

$$w_{t(d)}''(r) - \frac{6}{r^2} w_{t(d)}(r) - m_N (E - V_C(r) + 2V_T(r)) w_{t(d)}(r) = \sqrt{8}m_N V_T(r) u_{t(d)}(r). \quad (\text{A.3})$$

The equations for the parity-admixed states are

$$\tilde{v}_t^{3p0''}(r) - \frac{2}{r^2} \tilde{v}_t^{3p0} + m_N (E - V_C(r) + 4V_T(r)) \tilde{v}_t^{3p0} =$$

$$\begin{aligned}
& -2 \left[(\chi_\rho + 2) u_s(r) \frac{\partial}{\partial r} \left(F_\rho^0(r) - \sqrt{\frac{2}{3}} F_\rho^2(r) \right) + (\chi_\omega + 2) u_s(r) \frac{\partial}{\partial r} F_\omega^0(r) \right. \\
& \left. + 2r \left(F_\rho^0(r) - \sqrt{\frac{2}{3}} F_\rho^2(r) + F_\omega^0(r) \right) \frac{\partial}{\partial r} \left(\frac{u_s(r)}{r} \right) \right], \tag{A.4}
\end{aligned}$$

$$\begin{aligned}
& \tilde{v}_{t(d)}^{3p1''}(r) - \frac{2}{r^2} \tilde{v}_{t(d)}^{3p1}(r) + m_N (E - V_C(r) - 2V_T(r)) \tilde{v}_{t(d)}^{3p1}(r) = \\
& \frac{2}{\sqrt{3}} \left[\left(u_{t(d)}(r) + \frac{1}{\sqrt{2}} w_{t(d)}(r) \right) \frac{\partial}{\partial r} \left(F_\pi^1(r) + \sqrt{2} F_\rho^1(r) - \sqrt{2} F_\omega^1(r) - \sqrt{2} F_\rho^{1'}(r) \right) \right. \\
& \left. + 2\sqrt{2} (F_\rho^1(r) - F_\omega^1(r)) \frac{\partial}{\partial r} \left(u_{t(d)}(r) + \frac{1}{\sqrt{2}} w_{t(d)}(r) \right) \right. \\
& \left. - \frac{2\sqrt{2}}{r} (F_\rho^1(r) - F_\omega^1(r)) (u_{t(d)}(r) - \sqrt{2} w_{t(d)}(r)) \right], \tag{A.5}
\end{aligned}$$

$$\begin{aligned}
& \tilde{v}_d^{1p1''}(r) - \frac{2}{r^2} \tilde{v}_d^{1p1} + m_N (E - V_C(r)) \tilde{v}_d^{1p1} = \\
& \frac{2}{\sqrt{3}} \left[\left(u_d(r) - \sqrt{2} w_d(r) \right) \frac{\partial}{\partial r} \left(3\chi_\rho F_\rho^0(r) - \chi_\omega F_\omega^0(r) \right) \right. \\
& \left. - 2 (3F_\rho^0(r) - F_\omega^0(r)) \frac{\partial}{\partial r} (u_d(r) - \sqrt{2} w_d(r)) \right. \\
& \left. + \frac{2}{r} (3F_\rho^0(r) - F_\omega^0(r)) (u_d(r) + 2\sqrt{2} w_d(r)) \right], \tag{A.6}
\end{aligned}$$

where $F_M^{\Delta I}(r) \equiv g_{MNN} h_M^{\Delta I} f_M(r)$.

[1] C. S. Wood *et al.*, Science **275** (1997) 1759.

[2] S. C. Bennett and C. E. Wieman, Phys. Rev. Lett. **82** (1999) 2484.

[3] A. R. Berdoz *et al.*, Phys. Rev. Lett. **87** (2001) 272301.

[4] W. M. Snow *et al.*, Nucl. Instrum. Methods **440** (2000) 729.

[5] B. Desplanques, J. F. Donoghue and B. R. Holstein, Ann. Phys. **124** (1980) 449.

[6] E. G. Adelberger and W. C. Haxton, Ann. Rev. Nucl. Part. Sci. **35** (1985) 501.

[7] B. Desplanques, Phys. Rep. **297** (1998) 1.

[8] J. Alberi *et al.*, Can. J. Phys. **66** (1988) 542.

[9] B. Desplanques, Nucl. Phys. **A 242** (1975) 425.

[10] M. Lacombe, B. Loiseau, J. M. Richard, R. Vinh Mau, J. Côté, P. Pirés and R. de Tourreil, Phys. Rev. C **21** (1980) 861.

[11] R. Machleidt, K. Holinde and Ch. Elster, Phys. Rept. **149** (1987) 1.

- [12] R. Machleidt, Adv. Nucl. Phys. **19** (1989) 189.
- [13] R. B. Wiringa, V. G. J. Stoks and R. Schiavilla, Phys. Rev. C **51** (1995) 38.
- [14] B. A. Craver, E. Fischbach, Y. E. Kim and A. Tubis, Phys. Rev. D **13** (1976) 1376.
- [15] V. A. Knyazkov *et al.*, Nucl. Phys. **A 417** (1984) 209.
- [16] B. H. H. McKellar and K. R. Lassey, Phys. Rev. C **17** (1978) 842.
- [17] F. Pauss, L. Mathelitsch, J. Côté, M. Lacombe, B. Loiseau and R. Vinh Mau, Nucl. Phys. **A 365** (1981) 392.
- [18] R. Schiavilla, J. Carlson and M. Paris, Phys. Rev. C **70** (2004) 044007.
- [19] C. H. Hyun, T.-S. Park and D.-P. Min, Phys. Lett. **B 516** (2001) 321.
- [20] S. Morioka, P. Grange and Y. Avishai, Nucl. Phys. **A 457** (1986) 518.